Fluctuation effects in block copolymer melts

O. N. Vassiliev[a] and M. W. Matsen[b]
Polymer Science Centre, University of Reading, Whiteknights, Reading RG6 6AF, United Kingdom

(Received 13 November 2002; accepted 30 January 2003)

Fluctuation effects in symmetric diblock copolymer melts are quantitatively examined with the first direct comparison between Monte Carlo simulations and mean-field theory where both are performed on the same identical model. The simulations provide the most conclusive evidence to date that fluctuations transform the continuous mean-field order–disorder transition (ODT) into a discontinuous transition. Furthermore, the fluctuations shift the ODT toward high segregation, χN, by a factor of ~ 2.7, which is much greater than that suggested by the Fredrickson–Helfand fluctuation theory. For the range of small molecules examined in our study, this shift is nearly independent of molecular weight. In the disordered phase, we find the usual large deviations from mean-field theory, but we find no indication whatsoever that they set in abruptly at some well-defined temperature as previously claimed. © *2003 American Institute of Physics.*
[DOI: 10.1063/1.1562616]

I. INTRODUCTION

Due to a continuing emergence of applications combined with intriguing phase behavior, block copolymers have been the subject of considerable research.[1] Although many experimental observations are now well explained by mean-field theory, there are, however, a number of pivotal issues that remain unresolved.[2] In particular, we are still uncertain about the corrections to mean-field theory, referred to as fluctuation effects.[3] Furthermore, the inability[4] to assign a reliable temperature dependence to the Flory–Huggins χ parameter, used to model the molecular interactions, restricts our ability to experimentally test refinements to the theory.

Such fundamental issues are typically addressed by considering symmetric diblock copolymers, where the A and B blocks both have $N/2$ segments, each of volume ρ_0^{-1}, and statistical segment length a. Within mean-field theory, the standard Gaussian chain model[2] predicts a continuous transition of the Brazovskii[5] class at $\chi N=(\chi N)_{\mathrm{ODT}}^{\mathrm{mf}}=10.495$.[6] For $\chi N<10.495$, the melt forms a homogeneous disordered state, whereas for $\chi N>10.495$, the copolymers microphase separate into an ordered lamellar structure with thin alternating A- and B-rich layers. Fredrickson and Helfand[3] have proposed a fluctuation correction, which instead predicts a discontinuous order–disorder transition (ODT) at

$$(\chi N)_{\mathrm{ODT}}^{\mathrm{fluct}}=(\chi N)_{\mathrm{ODT}}^{\mathrm{mf}}+41\bar{N}^{-1/3}. \tag{1}$$

The magnitude of the correction is dependent upon an invariant polymerization index, $\bar{N}\equiv\rho_0^{-2}a^6N$, which reflects the degree of overlap among the polymer chains. The overlap occurs because a typical molecule spans a volume of $\sim a^3N^{3/2}$, whereas its actual molecular volume, N/ρ_0, is generally much smaller. Experimental values of $\bar{N}$ generally range from $\sim 10^3$ to $\sim 10^4$.[7] The conventional wisdom is that the overlap or superposition of molecules averages out fluctuation effects causing mean-field theory to become exact in the $\bar{N}\to\infty$ limit.

The Fredrickson–Helfand fluctuation correction has gone relatively unquestioned for 15 years, even though it relies on debatable assumptions.[2,8] Unfortunately, experimental tests of Eq. (1) are complicated by the fact that the Flory–Huggins χ parameter used by block copolymer theories possesses an unknown temperature dependence. In many cases, $\chi(T)$ is determined experimentally by measuring the temperature of $(\chi N)_{\mathrm{ODT}}$ for several values of $\bar{N}$, and then fitting to Eq. (1). Unfortunately, this compromises any attempt to test the F–H fluctuation theory. The same applies when $\chi(T)$ is derived from the disordered-state scattering function as this also relies on a fit to the F–H theory. Maurer *et al.*[4] circumvented this problem by instead extracting $\chi(T)$ from a chemically-equivalent homopolymer blend, and, in doing so, found Eq. (1) to be highly inaccurate. They suggested a possible remedy to the block copolymer theory, but it resulted in the unprecedented prediction that $(\chi N)_{\mathrm{ODT}}^{\mathrm{fluct}}<(\chi N)_{\mathrm{ODT}}^{\mathrm{mf}}$.

The most reliable way of assessing fluctuation effects would seem to be a direct comparison between mean-field theory and Monte Carlo simulations.[9] Indeed, the initial Monte Carlo studies by Fried and Binder[10–12] have detected nonmean-field behavior, such as chain stretching and the onset of microdomain formation, deep within the disordered phase. While most simulations[10–15] indicate that the nonmean-field behavior grows in slow and continuously, Pakula *et al.*[16] provided evidence that it occurs abruptly at $\chi N\approx 0.7(\chi N)_{\mathrm{ODT}}$. Despite the ability of Monte Carlo methods to successfully address such issues, they have encountered significant complications.

The majority of Monte Carlo simulations have failed to detect the ODT by direct means, even though, according to both theory[3] and experiment,[17] it is a discontinuous transition that should, in general, produce a spike in the heat capacity

[a]Electronic mail: ovassil@mail.mdanderson.org
[b]Electronic mail: m.w.matsen@reading.ac.uk

and discontinuities in all thermodynamic quantities. Fried and Binder[10–12] were forced to estimate the ODT according to a somewhat arbitrary criterion involving the relaxation time of the melt composition. Weyersberg and Vilgis[18] observed a peak in the specific heat of their simulations, but it appeared to be rather broad and was highly obscured by their statistical noise. With much improved statistics, Hoffmann *et al.*[13] concluded that the heat capacity was continuous near the ODT. In those studies,[13,14] they could only estimate the ODT by the appearance of high-order peaks in the structure function. Larson[19] estimated the ODT by examining the segment profile as a preprepared lamellar morphology was heated above the ODT, but he did not examine any other thermodynamic quantities that might corroborate his predictions. Micka and Binder[15] attempted to locate the ODT using finite-scaling methods appropriate to continuous and weakly discontinuous transitions, but they were unsuccessful. They attributed this to complicated finite-size effects owning to the fact that the periodicity of the ordered phase is constrained to be commensurate with the simulation box. More recently, there has emerged some Monte Carlo evidence that the ODT is discontinuous. Dotera and Hatano[20] have observed a discontinuous jump in the internal energy and in the average end-to-end length of the molecules. Pakula *et al.*[16] have also detected a small discontinuity in the molecular size and the internal energy along with a corresponding spike in the heat capacity. However, neither study investigated the transition thoroughly.

Another complication is that mean-field calculations[2] generally apply the coarse-grained Gaussian chain model treating polymer chains as thin elastic threads of constant volume,[2] whereas Monte Carlo simulations generally employ lattice models in which among other things chains are not coarse grained (at least not in the same sense). Naturally, we cannot expect the models to be equivalent, particularly for the short chain lengths considered by the simulations (i.e., $\bar{N} \lesssim 10^2$). As a consequence, it is uncertain to what degree the differences between mean-field theory and Monte Carlo simulations are due to fluctuation effects as opposed to variations in the underlying models. The problem is particularly acute when attempting[10,18,19] to test Eq. (1), because of the ambiguity[21] resulting from the model dependence of χ. The obvious solution is to perform either the Monte Carlo simulations on the continuum coarse-grained model or the mean-field calculations on a lattice model. There have been recent attempts to develop Monte Carlo simulations for the continuum model,[22] but these methods are very numerically demanding and there remain outstanding theoretical issues still to be resolved. On the other hand, Scheutjens and Fleer[23] have developed the mean-field theory for lattice models some time ago. Therefore, we choose the second option.

Below we perform Monte Carlo simulations and mean-field calculations on the same identical lattice model so as to provide completely unbiased comparisons. The lattice model we choose is the same as that in the Monte Carlo simulations of Pakula *et al.*[16] However, contrary to their initial study, we find that the nonmean-field behavior does not emerge abruptly at a well-defined temperature, but we do find the ODT to be clearly discontinuous. Whereas the original study by Pakula *et al.*[16] was limited to a single relatively small system size, we examine a range of significantly larger systems allowing us to assess the finite-size effects. We find that they are not so overwhelming as Ref. 15 might suggest, and thus we are able to estimate the ODT with reasonable accuracy. When we compare this to mean-field theory, we are surprised to find that $(\chi N)_{\mathrm{ODT}}^{\mathrm{fluct}} \approx 2.7 (\chi N)_{\mathrm{ODT}}^{\mathrm{mf}}$ with no indication that this discrepancy diminishes with increasing molecular weight.

II. MONTE CARLO SIMULATIONS

This section describes our Monte Carlo simulations for a lattice model containing n AB diblock copolymer molecules. Each molecule is a linear sequence of N monomers, which are labeled $s=1,2,\ldots,N$. Those labeled as $s=1,2,\ldots,N_A$ are designated as A-type monomers, while the remaining $N_B \equiv N-N_A$ are B-type monomers. The copolymer chains are all placed on a lattice with no more than one monomer per site and with each pair of bonded monomers occupying nearest-neighbor sites. Here we use a cubic $L\times L\times L$ lattice of V sites and a lattice constant of d. The allowed lattice vectors are given by $\mathbf{r}_i = d(h,k,l)$, where $i=1,2,\ldots,V$ labels the different sites and h, k, and l are integers ranging from 1 to L. By only permitting sites where $h+k+l$ equals an even integer, we obtain an fcc lattice with $V=L^3/2$ sites, where the bond length is $b=\sqrt{2}d$. The fcc lattice is chosen for its large coordination number, $z=12$, so as to minimize artifacts associated with the discrete nature of the lattice. Furthermore, we employ periodic boundary conditions in an effort to minimize finite-size effects. Note that these boundary conditions require L to be even.

To operate effectively, our algorithm allows some room for the polymers to move by partially filling the lattice to an average copolymer occupancy of $\phi_c \equiv nN/V \approx 0.8$. Ideally, we would prefer to consider the $\phi_c = 1$ limit as Pakula *et al.*[16] have done, but this would require a more complex and computationally demanding algorithm, which would significantly restrict our system size. Ultimately, we are persuaded by arguments of Binder *et al.*[11,15] that vacancies tend to follow the dilution approximation[24] imparting on the system nothing more than a small degree of compressibility, which real melts possess anyway. In any case, we will perform our mean-field calculations with the exact same vacancy concentration.

For convenience, we specify the occupancy of the ith site using a pseudo-spin variable, σ_i, that takes on the values 1, 0, or -1 depending if the site contains an A monomer, vacancy, or B monomer, respectively. This allows us to specify the Hamiltonian for our system as

$$\frac{H}{k_B T} = \frac{1}{4} \sum_{\langle ij \rangle} [(\epsilon_{AA} - 2\epsilon_{AB} + \epsilon_{BB})\sigma_i \sigma_j + (\epsilon_{AA} + 2\epsilon_{AB} + \epsilon_{BB}) \times \sigma_i^2 \sigma_j^2 + (\epsilon_{AA} - \epsilon_{BB})\sigma_i \sigma_j (\sigma_i + \sigma_j)], \quad (2)$$

where the sum is over all nearest-neighbor sites. The quantity $\epsilon_{\alpha\beta}$ is interpreted as the interaction energy between two neighboring monomers of type α and β, and is related to the Flory–Huggins parameters,

$$\chi_{\alpha\beta} \equiv \frac{z\epsilon_{\alpha\beta}}{k_B T}. \tag{3}$$

Although this definition of $\chi_{\alpha\beta}$ is typical of lattice mean-field calculations, Monte Carlo simulations often employ somewhat different definitions,[21] where, for example, z is replaced by $(z-2)\phi_c$.[10,16] This, in fact, represents one of the major ambiguities that exists when trying to compare lattice-based results to predictions, such as Eq. (1), derived from a continuum course-grained model where the issue of coordination number does not exist. However, in our case where everything is performed on the same lattice model, this ambiguity is completely avoided. For example, if we used the alternative definition mentioned above, then all our χ values would be reduced by a factor of 2/3, but the eventual conclusion that our Monte Carlo and mean-field predictions of $(\chi N)_{\mathrm{ODT}}$ differ by a factor of ~ 2.7 would still hold.

It turns out that the effects of the three $\chi_{\alpha\beta}$ parameters are not independent. In fact, the behavior of the system is primarily controlled by the single quantity,

$$\chi \equiv \chi_{AB} - \tfrac{1}{2}(\chi_{AA} + \chi_{BB}), \tag{4}$$

provided the number of vacancies is low. This is because the sum of the last two terms in Eq. (2) produces an irrelevant constant in the limit of $\phi_c \to 1$. Thus, without any significant loss of generality, we choose $\chi_{AA} = \chi_{BB} = 0$.

Our Monte Carlo simulations are based on the standard Metropolis algorithm.[25] At each Monte Carlo step (MCS), an attempt is made to change the configuration of the system by altering one or two of the copolymers. If the potential move results in the double occupancy of a site, it is immediately rejected. Otherwise, we proceed to calculate the resulting energy change, $\Delta E \equiv H_{\mathrm{final}} - H_{\mathrm{initial}}$, using Eq. (2). If the move reduces the overall energy of the system (i.e., $\Delta E < 0$) then it is automatically accepted, and if it increases the energy then it is accepted with a probability of $\exp(-\Delta E/k_B T)$.

The efficiency of a Monte Carlo algorithm relies on having a good selection of potential moves so that the configuration of the system can evolve as rapidly as possible. The computation time required to assess each move should be small and the acceptance rate should be high. Furthermore, the variety of moves should be sufficient to allow all aspects of the system to relax. At each MCS, we randomly choose among four types of moves using predefined probabilities, which we select later in Sec. IV B. Since we are only concerned with equilibrium behavior, we allow unphysical moves, which implies that we cannot associate any significance to our Monte Carlo dynamics. Examples of each move are shown in Fig. 1.

The first type of MCS is the standard slithering snake move.[10,11,15] It is performed by randomly selecting one of the $2n$ chain ends in the system, along with one of its $z = 12$ nearest-neighbor sites. The algorithm then tries to move the chain end to the selected site, by shifting all the monomers in the chain one site along the contour of the chain. Normally, this move can only be performed if the selected site is vacant. The one exception is when the site is occupied by the other end of the moving chain.

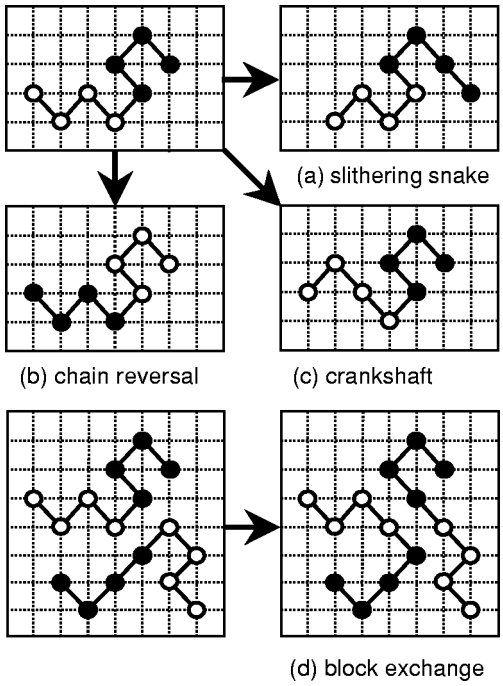

FIG. 1. Examples of our four Monte Carlo moves: (a) slithering snake, (b) chain reversal, (c) crankshaft, and (d) block exchange. For clarity, the examples are shown for a short ($N = 8$) diblock constrained to the x–y plane.

Our algorithm also permits a polymer to perform a complete chain reversal (i.e., head-to-tail flip).[10,11,15] This MCS randomly chooses one of the n chains in the system, and then considers the possibility of interchanging the s and $N-s$ monomers for all $s = 1$ to $N/2$. Note that such moves can never be rejected on the basis of double occupancy.

We also allow for crankshaft moves. This MCS chooses one of the $n(N-2)$ nonend monomers in the system, and tries to move it, while keeping its two bonded neighbors fixed. The number of potential moves is 0, 1, 3, or 3, depending on whether the bond angle is 180°, 120°, 90°, or 60°, respectively. In the first case, no move is performed, while in either of the latter two cases, we choose randomly among the three possibilities.

The final type of move involves the exchange of blocks between two nearby copolymers. This attempt begins by randomly selecting one of the n block copolymer junctions in the system. Next we count the number of nearby junctions which would allow the exchange of their blocks without actually moving any monomers. One of these is chosen randomly unless none exist, in which case the system remains unchanged. Note that any exchange will always be accepted since $\Delta E = 0$.

Using the algorithm described above, we perform simulations for various combinations of chain length, N, and system size, L. In each case, the simulation starts in the disordered phase at $\chi = 0$ and steps up in small increments, $\Delta\chi$, until the system has formed a well-ordered lamellar phase. Then we reverse the direction and run the simulation past the ODT returning to the disordered phase. Immediately following each increment in χ, we run the simulation for a sufficient period of time (typically, 4×10^4 MCS per monomer) to allow the system to relax back to equilibrium. At the very

beginning (i.e., $\chi=0$), we allow an extra long relaxation period, due to the fact we start from a highly artificial state with the polymers extended so that the lattice can be easily filled to the desired level (i.e., $\phi_c=0.8$). After each relaxation period, we collect statistics for the purpose of evaluating various thermodynamic averages. For example, we calculate the internal energy using $U=\langle H\rangle$ and the heat capacity using

$$C_V \equiv \frac{\partial U}{\partial T} = \frac{\langle H^2\rangle - U^2}{k_B T^2}, \tag{5}$$

where the angular brackets denote averages over a sequence of Monte Carlo configurations at fixed χ. Typically, the sequence involves 4×10^4 MCS per monomer, from which we sample one configuration every 20 MCS per monomer. Naturally, we have performed test runs to confirm that the numbers of Monte Carlo steps used for equilibriating and for collecting statistics are both sufficient. We are further assured of this by the fact that our cooling and heating runs provide consistent results.

In order to monitor the average configuration of an individual polymer molecule, we evaluate the radii of gyration, R_g, $R_{g,\mathrm{A}}$, and $R_{g,\mathrm{B}}$, for an entire molecule, an A block, and a B block, respectively. Their exact definitions are given by

$$R_g^2 = \frac{1}{N}\sum_{s=1}^{N} \langle |\mathbf{r}_s - \mathbf{R}_{\mathrm{cm}}|^2\rangle, \tag{6}$$

$$R_{g,\mathrm{A}}^2 = \frac{1}{N_A}\sum_{s=1}^{N_A} \langle |\mathbf{r}_s - \mathbf{R}_{\mathrm{cm,A}}|^2\rangle, \tag{7}$$

$$R_{g,\mathrm{B}}^2 = \frac{1}{N_B}\sum_{s=N_A+1}^{N} \langle |\mathbf{r}_s - \mathbf{R}_{\mathrm{cm,B}}|^2\rangle, \tag{8}$$

where $\mathbf{r}_s$ specifies the position of the sth monomer, and

$$\mathbf{R}_{\mathrm{cm}} = \frac{1}{N}\sum_{s=1}^{N} \mathbf{r}_s, \tag{9}$$

$$\mathbf{R}_{\mathrm{cm,A}} = \frac{1}{N_A}\sum_{s=1}^{N_A} \mathbf{r}_s, \tag{10}$$

$$\mathbf{R}_{\mathrm{cm,B}} = \frac{1}{N_B}\sum_{s=N_A+1}^{N} \mathbf{r}_s, \tag{11}$$

define the centers of mass. We also evaluate the additional parameter,

$$R_{\mathrm{AB}}^2 = \langle |\mathbf{R}_{\mathrm{cm,A}} - \mathbf{R}_{\mathrm{cm,B}}|^2\rangle, \tag{12}$$

to measure for the average separation between the A and B blocks of a molecule.

To quantify the overall structure of the system, we calculate the spin–spin correlation function,

$$G_{ij} = \langle \sigma_i \sigma_j\rangle - \langle \sigma_i\rangle^2, \tag{13}$$

where $i,j=1,2,\ldots,V$. [Note that $\langle \sigma_i\rangle = \phi_c(N_A-N_B)/N$.] From the correlation function, we can also evaluate the structure function,

$$S(\mathbf{q}) = \frac{1}{V}\sum_{ij} G_{ij} \exp[i\mathbf{q}\cdot(\mathbf{r}_i - \mathbf{r}_j)], \tag{14}$$

which corresponds to the pattern observed in a small-angle scattering experiment. Because our simulation box is finite, the wave vector is only permitted to take on a discrete set of values: $\mathbf{q}=2\pi(h,k,l)/Ld$, where h, k, and l are integers.

Ideally, the ODT can be identified by monitoring an appropriate order parameter that switches from zero to nonzero when the disordered phase transforms into the lamellar phase. However, the fact that the lamellar phase emerges with an unspecified period and orientation renders simple definitions based on the segment profile ineffective. After some investigation, we found that

$$\psi = \frac{1}{V^2}\sum_{i\neq j} G_{ij}^2 \tag{15}$$

serves as an excellent order parameter. In the disorder phase, the sum of G_{ij}^2 scales as the volume of the system, V, whereas in the ordered phase, it scales as V^2 provided the long-range order extends over the entire system. Consequently, ψ assumes a small positive value in the disordered phase that approaches zero for large system sizes, and it exhibits a reasonably large value in the ordered phase that is roughly independent of system size. Although ψ is not identically zero in the disordered state, it does possess the most important property of an order parameter in that it is highly sensitive to the ODT.

To optimize the dynamics of our Monte Carlo algorithm, we tune the attempt rates for the four moves shown in Fig. 1. This is done by examining the spin and density autocorrelation functions,

$$G_\sigma(t) = \langle \sigma_i(t')\sigma_i(t'+t)\rangle - \langle \sigma_i\rangle^2, \tag{16}$$

$$G_\rho(t) = \langle \sigma_i^2(t')\sigma_i^2(t'+t)\rangle - \langle \sigma_i^2\rangle^2, \tag{17}$$

respectively. (Note that $\langle \sigma_i^2\rangle = \phi_c$.) Here t and t' denote time measured in terms of MCS per monomer. We also monitor the acceptance rates for each of the four moves. The resulting choice of attempt rates is discussed in Sec. IV B.

III. MEAN-FIELD THEORY

This section presents the mean-field theory for the identical lattice model following a formalism similar to that of Scheutjens and Fleer.[23] Assuming that the ordered phase at large χN is a lamellar structure, we divide the lattice into $M_\perp$ sequentially numbered layers each with $M_\parallel$ sites. Furthermore, we define λ_δ to specify the fraction of nearest-neighbor sites in layer $(i+\delta)$ for a given site in layer i. For a lamellar phase oriented normal to the (111) direction, $M_\perp = L/2$, $M_\parallel = L^2$, $\lambda_0 = \frac{1}{2}$, and $\lambda_1 = \lambda_{-1} = \frac{1}{4}$, where as for lamellae in the (100) direction, $M_\perp = L$, $M_\parallel = L^2/2$, and $\lambda_0 = \lambda_1 = \lambda_{-1} = \frac{1}{3}$. In both cases, $\lambda_\delta = 0$ for $|\delta| > 1$. In mean-field theory, there is no advantage of having a large lattice, and so $M_\perp$ (i.e., L) is chosen to contain a single period of the lamellar phase. Provided that we select the size (i.e., lamellar period) that minimizes the free energy, our results will nevertheless correspond to the thermodynamic limit of $L\to\infty$.

Since mean-field theory is only sensitive to the average concentration of A and B monomers in each layer, we group the configurations of individual polymers according to the layers in which their monomers occur. This permits us to define a function, $k(c,s)$, specifying the layer of the sth monomer for all polymers in the configuration group c. Then, within the mean-field approximation, the average interaction energy between a pair of copolymers in configurations c and c' is

$$K_{cc'} \equiv \frac{z}{M_\parallel} \sum_{\alpha,\beta} \epsilon_{\alpha\beta} \sum_{i,i'} \lambda_{(i'-i)} r_{\alpha,c,i} r_{\beta,c',i'}, \tag{18}$$

where

$$r_{\alpha,c,i} = \sum_{s=1}^{N} \delta_{\alpha,\gamma(s)} \delta_{i,k(c,s)} \tag{19}$$

is the number of α-type monomers in layer i resulting from a single polymer in configuration group c, and

$$\gamma(s) = \begin{cases} A, & \text{if } 1 \leqslant s \leqslant N_A, \\ B, & \text{if } N_A + 1 \leqslant s \leqslant N. \end{cases} \tag{20}$$

This allows the average internal energy of the system to be written as

$$U(\{n_c\}) = \frac{1}{2} \sum_{c,c'} K_{cc'} n_c n_{c'}, \tag{21}$$

where n_c is the total number of polymers in configuration group c.

To proceed, we need to count the total number of states for a given set of occupation numbers, $\{n_c\}$. We start with the number of possible configurations,

$$\Omega_c \equiv M_\parallel z^{N-1} \prod_{s=2}^{N} \lambda_{k(c,s)-k(c,s-1)} \equiv M_\parallel z^{N-1} \omega_c, \tag{22}$$

of a single nonavoiding polymer in group c. Then, in terms of this, the number of states for the entire system is approximately

$$\Omega(\{n_c\}) = \left(\prod_c \frac{\Omega_c^{n_c}}{n_c!} \right) \frac{(M_\parallel!)^{M_\perp}}{M_\parallel^n \Pi_i \ell_i!}. \tag{23}$$

The first factor in the brackets is the number of states if the restriction of single occupancy per lattice site is lifted, while treating the polymers as indistinguishable. The remaining factors represent a mean-field correction for the single occupancy constraint. It is calculated by noting that the first time a segment is placed in layer i, there are $M_\parallel$ sites to choose from. The next time, there are $(M_\parallel - 1)$ sites, and so on until the final monomer has only $(\ell_i + 1)$ sites to choose from, where

$$\ell_i \equiv M_\parallel - \sum_c n_c (r_{A,c,i} + r_{B,c,i}) \tag{24}$$

is the number of vacancies in layer i.

The partition function is expressed in terms of the above quantities as

$$Z = \sum_{\{n_c\}} \Omega(\{n_c\}) \exp[-U(\{n_c\})/k_B T]. \tag{25}$$

In the thermodynamic limit, the sum is dominated by a single term determined by maximizing $\Omega \exp[-U/k_B T]$ under the constraint $\Sigma_c n_c = n$. This requires

$$n_c = \frac{V \omega_c}{Q} \prod_{i=1}^{M_\perp} (P_{A,i})^{r_{A,c,i}} (P_{B,i})^{r_{B,c,i}} \tag{26}$$

$$= \frac{V \omega_c}{Q} \prod_{s=1}^{N} P_{\gamma(s),k(c,s)}, \tag{27}$$

where Q serves as a Lagrange multiplier for the constraint, and

$$P_{\alpha i} \equiv \frac{\ell_i}{M_\parallel} \exp[-\chi_{\alpha A} \overline{\phi}_{A,i} - \chi_{\alpha B} \overline{\phi}_{B,i}] \tag{28}$$

is referred to as the *free segment probability* of component α in layer i. To evaluate $P_{\alpha,i}$, we need

$$\overline{\phi}_{\alpha,i} \equiv \sum_\delta \lambda_\delta \phi_{\alpha,i+\delta}, \tag{29}$$

where

$$\phi_{\alpha,i} \equiv \frac{1}{M_\parallel} \sum_c n_c r_{\alpha,c,i} = \sum_{s=1}^{N} \phi_{s,i} \delta_{\alpha,\gamma(s)} \tag{30}$$

is the volume fraction of α in layer i. This is expressed in terms of volume fraction of segment s in layer i,

$$\phi_{s,i} \equiv \frac{1}{M_\parallel} \sum_c n_c \delta_{i,k(c,s)} \tag{31}$$

$$= \frac{1}{M_\parallel} \sum_c \omega_c \delta_{i,k(c,s)} \prod_{t=1}^{N} P_{\gamma(t),k(c,t)} \tag{32}$$

$$= \frac{V p(s,i) q(s,i)}{Q P_{\gamma(s),i}}, \tag{33}$$

which requires two intermediate functions. The first is defined as

$$p(s,i) \equiv \sum_d \omega_d \delta_{i,k(d,s)} \prod_{t=1}^{s} P_{\gamma(t),k(d,t)} \tag{34}$$

$$= P_{\gamma(s),i} \sum_\delta \lambda_\delta p(s-1, i+\delta), \tag{35}$$

where the sum is over all configuration groups, d, of monomers 1 to s. Here, ω_d has an analogous definition to ω_c in Eq. (22), but where the product only involves the first s monomers. In practice, $p(s,i)$ is evaluated by using the recursive relation, Eq. (35), starting with $p(1,i) = P_{A,i}$. Similarly,

$$q(s,i) \equiv \sum_d \omega_d \delta_{i,k(d,s)} \prod_{t=s}^{N} P_{\gamma(t),k(d,t)} \tag{36}$$

$$= P_{\gamma(s)i} \sum_\delta \lambda_\delta q(s+1, i+\delta) \tag{37}$$

involves a sum over configuration groups for the monomers from s to N, and is evaluated recursively starting with $q(N,i)=P_{B,i}$. The Lagrange multiplier is evaluated by

$$\frac{Q}{V}=\frac{N}{\phi_c M_\perp}\sum_{i=1}^{M_\perp}\frac{p(s,i)q(s,i)}{P_{\gamma(s),i}}, \tag{38}$$

which yields a result independent of s.

Our numerical procedure for finding a solution to the above equations begins with an initial guess for the profiles, $\phi_{A,i}$ and $\phi_{B,i}$. From that, we evaluate $\overline{\phi}_{A,i}$, $\overline{\phi}_{B,i}$, and $\ell_i/M_\parallel=1-\phi_{A,i}-\phi_{B,i}$. Next, $P_{A,i}$ and $P_{B,i}$ are evaluated, which allows us to calculate $p(s,i)$ and $q(s,i)$. Then, we calculate $\phi_{s,i}$, which returns values for $\phi_{A,i}$ and $\phi_{B,i}$. Of course, these profiles will differ from our initial guess, but this is easily remedied by adjusting the initial guess with a quasi-Newton–Raphson technique until a self-consistent solution is achieved.

There will, in general, be multiple solutions (e.g., different lamellar periods), and to determine the stable one we need to evaluate their free energies, $F\equiv -k_BT\ln Z=U(\{n_c\})-k_BT\ln\Omega(\{n_c\})$. By using Eq. (27) for n_c and making use of the constraint on $\Sigma_c n_c$, we obtain

$$\frac{F}{nk_BT}=\frac{N}{\phi_c M_\perp}\sum_{i=1}^{M_\perp}\left(\ln\left(\frac{\ell_i}{M_\parallel}\right)-\frac{1}{2}\sum_{\alpha,\beta}\chi_{\alpha\beta}\phi_{\alpha,i}\overline{\phi}_{\beta,i}\right)-\ln\left(\frac{Q}{V}\right), \tag{39}$$

to within irrelevant constants. In the disordered phase, this reduces to

$$\frac{F_D}{nk_BT}=\frac{(1-\phi_c)N}{\phi_c}\ln(1-\phi_c)+\frac{\phi_c N}{2}[2\chi_{AB}f(1-f)+\chi_{AA}f^2+\chi_{BB}(1-f)^2], \tag{40}$$

where $f=N_A/N$ is the fraction of A monomers in each copolymer.

IV. RESULTS

Below, we investigate our lattice model for symmetric diblocks (i.e., $f=0.5$) of $N=20$, 30 and 40 each over a range of system sizes, L. In all cases, we choose an occupation level of $\phi_c=0.8$. Furthermore, we select $\chi_{AA}=\chi_{BB}=0$, which proves to be appropriate in that the vacancies remain well mixed and uniformly distributed throughout the system.

A. Mean-field theory

We start by investigating mean-field theory as this will provide valuable guidance for our subsequent Monte Carlo study. Within mean-field theory, the disordered phase is unaffected by changes in χN. For instance, the average number of A/B monomer contacts remains fixed at

$$\langle n_{AB}\rangle=zV\phi_c^2 f(1-f), \tag{41}$$

which implies that the internal energy, U, is temperature independent. From this, it follows that the heat capacity, C_V, is identically zero. Furthermore, the diblocks obey random-walk statistics throughout the entire disordered phase, which implies that the average molecular dimensions are fixed at

$$R_g^2=\frac{b^2N}{6}\left(1-\frac{1}{N^2}\right)\approx\frac{b^2N}{6}, \tag{42}$$

$$R_{g\mathrm{A}}^2=\frac{b^2N_\mathrm{A}}{6}\left(1-\frac{1}{N_\mathrm{A}^2}\right)\approx\frac{b^2N_\mathrm{A}}{6}, \tag{43}$$

$$R_{g\mathrm{B}}^2=\frac{b^2N_\mathrm{B}}{6}\left(1-\frac{1}{N_\mathrm{B}^2}\right)\approx\frac{b^2N_\mathrm{B}}{6}, \tag{44}$$

$$R_{\mathrm{AB}}^2=\frac{b^2N}{3}\left(1+\frac{1}{2N_\mathrm{A}N_\mathrm{B}}\right)\approx\frac{b^2N}{3}. \tag{45}$$

These molecular dimensions are obtained following Ref. 26, and, as pointed out in Refs. 10 and 12, they satisfy the condition, $R_{\mathrm{AB}}^2\approx 2R_g^2$.

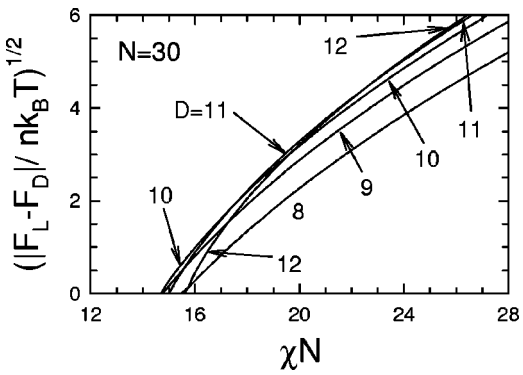

FIG. 2. Free energy difference between the lamellar and disordered phases, F_L-F_D, as a function of segregation, χN, calculated by mean-field theory for diblocks of $N=30$ monomers each. The different curves correspond to lamellae in the (111) orientation with periods ranging from $D=8$ to 12 layers. The square root is plotted to better emphasize the location of the ODT.

The lamellar phase, however, does respond to increases in χN by reducing $\langle n_{\mathrm{AB}}\rangle$, and consequently it becomes stable at low temperatures. Figure 2 plots the difference between the lamellar and disordered state free energies as a function of χN for symmetric diblocks with $N=30$. The various curves correspond to lamellae of different periods D, but all with the same (111) orientation. In this case, the disordered phase first becomes unstable to the $D=10$ lamellar phase at $(\chi N)_{\mathrm{ODT}}=14.668$. Notice that within just one unit of χN, the disordered phase is unstable to a wide range of other lamellar periods (i.e., $8\leqslant D\leqslant 12$), which, as we will discuss later, implies that our Monte Carlo simulations should not be too seriously affected by finite-size effects. If we repeat the mean-field calculation for lamellae in the (100) direction, the ODT shifts ever so slightly to $(\chi N)_{\mathrm{ODT}}=14.654$. Although the difference in the two values is inconsequential, we should in principle use the lower one as our ODT. Results for the other degrees of polymerization, N, are summarized in Table I. From those, we see that the mean-field ODT of our lattice model has a sizable molecular-weight dependence and that the location differs significantly from that of the continuum Gaussian chain model, which predicts $(\chi N)_{\mathrm{ODT}}=10.495/\phi_c=13.119$ irrespective of the molecular weight.[24]

TABLE I. Mean-field theory ODT's and corresponding lamellar periods for three degrees of polymerization, N, and two lamellar orientations.

	(111) direction		(100) direction	
N	D_{ODT}	$(\chi N)_{\mathrm{ODT}}$	D_{ODT}	$(\chi N)_{\mathrm{ODT}}$
20	8	15.3	10	15.4
30	10	14.7	11	14.7
40	11	14.3	13	14.3

The A-segment and vacancy profiles, $\phi_{\mathrm{A},i}$ and $\phi_{V,i}$, respectively, are plotted in Fig. 3 for $N=30$ and a (111) lamellar orientation. As the ODT is crossed, the oscillation in the A-segment profile grows from zero signifying that the mean-field ODT is continuous. Furthermore, the period of the lamellar phase increases with segregation. On the basis of Fig. 2, the period switches from $D=10$ to 11 at $\chi N=17.38$ and then to $D=12$ at $\chi N=22.57$. Also notice that the distribution of vacancies remains relatively uniform even at high χN, confirming that we have chosen appropriate values for χ_{AA} and χ_{BB}.

B. Optimizing the Monte Carlo algorithm

Before performing the bulk of our Monte Carlo simulations, we adjust the probabilities assigned to our four Monte Carlo moves to maximize the efficiency of our algorithm. We are guided by the acceptance rate for each move and the two autocorrelation functions, $G_\sigma(t)$ and $G_\rho(t)$, plotted in Fig. 4. In particular, we look for high acceptance rates and short relaxation times, τ_σ and τ_ρ, defined by $G_\sigma(\tau_\sigma)=\frac{1}{2}G_\sigma(0)$ and $G_\rho(\tau_\rho)=\frac{1}{2}G_\rho(0)$. However, these are not sufficient conditions for an efficient algorithm, and thus we must supplement these quantitative measures with some degree of judgement. We also focus more on low temperatures as this is where the Monte Carlo dynamics tend to be slowest.

The slithering snake step is among the most highly used moves for polymeric systems, and is associated with a fast center-of-mass diffusion.[10] It has a high acceptance rate even at low temperatures and a favorable effect on both τ_σ and τ_ρ. Although many algorithms rely almost entirely or even exclusively on this particular move,[10–12,15] we set its attempt rate at a modest 60%. Without alternative moves, the diffusion of the junction points would tend to cease once microphase separation occurred.

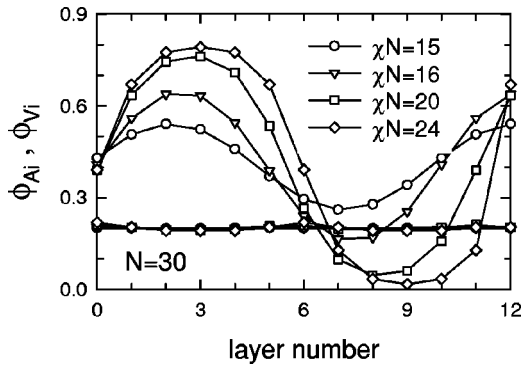

FIG. 3. Concentration profiles of A monomers and vacancies calculated by mean-field theory for diblocks of $N=30$ monomers and a (111) lamellar orientation. The vacancy profiles can be distinguished by the fact that $\phi_{V,i}\approx 0.2$.

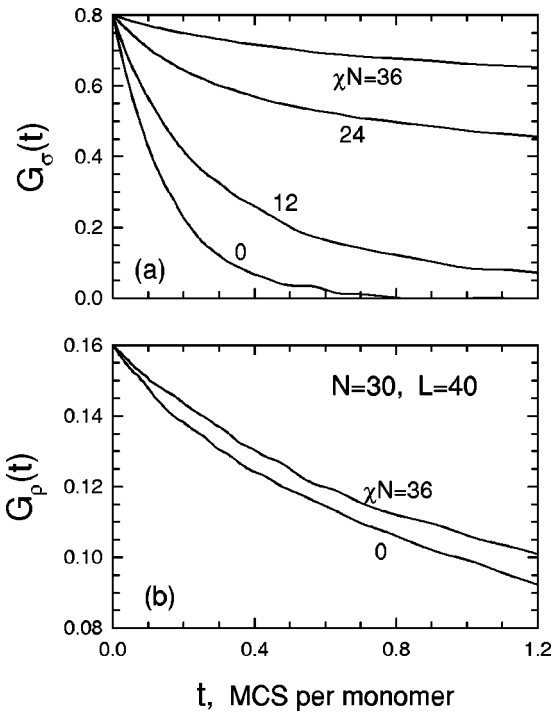

FIG. 4. Autocorrelation functions, $G_\sigma(t)$ and $G_\rho(t)$, vs Monte Carlo steps per monomer evaluated for a range of segregations. The simulations are all performed for diblocks of $N=30$ monomers on a lattice of size $L=40$.

At high temperatures, chain reversal has an acceptance rate of nearly 100% and it reduces τ_σ dramatically. However, the acceptance rate and the favorable effect on τ_σ drops off quickly as microphase separation sets in. Still, it is a useful move with a low execution cost, and so we assign it an attempt rate of 10%.

The crankshaft move has a reasonable acceptance rate even at low temperatures, and is effective at reducing τ_ρ. We also expect it to be one of the more effective moves for relaxing the central portion of the chain, especially once microphase separation sets in. Therefore, we give it a significant attempt rate of 20%.

Although the exchange of blocks tends to have the lowest acceptance rate ($\approx$5%), it has the merit of performing best at low temperatures where the junction points are concentrated at the A/B interfaces of highly-segregated morphologies. This move has little influence on τ_σ and τ_ρ, but we suspect that these are not good indicators of its effectiveness. We believe that this move is key for the lateral diffusion of chains along well-developed interfaces, and therefore we assign it an attempt rate of 10%.

The autocorrection functions shown in Fig. 4 are calculated for a series of segregations using our final selection of attempt rates. Under these conditions, the density autocorrection function, $G_\rho(t)$, displays a weak dependence on χN with a more or less constant relaxation time of $\tau_\rho\approx 1$ MCS per monomer. On the other hand, the spin autocorrection function, $G_\sigma(t)$, depends strongly on segregation with a re-

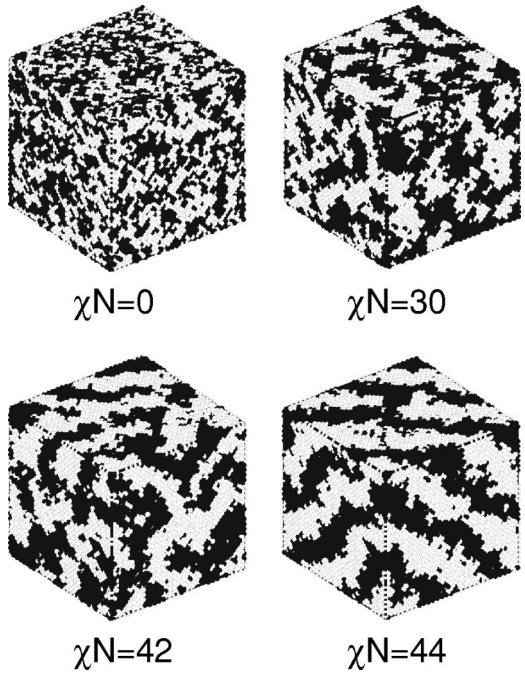

FIG. 5. Configurations taken at $\chi N=0$, 30, 42, (disordered) and 44 (lamellar) from a Monte Carlo cooling run involving diblocks of $N=30$ monomers on a lattice of size $L=60$. The two monomer types are distinguished by dark and light circles, while the vacancies are omitted.

laxation time that increases steadily from $\tau_\rho \approx 0.1$ MCS per monomer at $\chi N=0$.

C. Locating the ODT

The location of the ODT has been elusive in previous Monte Carlo studies.[10–15] The reason for this can be understood by examining the sequence of configurations shown in Fig. 5. The onset of microphase separation is such a gradual process that it is challenging to identify any significant differences between the disordered state at $\chi N=42$ and the ordered lamellar state at $\chi N=44$ apart from the long-range order present in the latter configuration. Not surprisingly, thermodynamic quantities tend to be insensitive to the ODT, but fortunately, our proposed order parameter, ψ, defined in Eq. (15) is an exception.

Figure 6 shows the variation in ψ for temperature scans back and forth across the ODT at three different molecular weights. In the disordered state ψ is tiny, while in the lamellar phase it increases by orders of magnitude. The fact that ψ displays a sharp jump indicates a discontinuous ODT, and indeed this is confirmed by the hysteresis loops. The widths of the hysteresis loops are recorded in Table II for four different system sizes at each of the three molecular weights. As expected, the widths tend to increase for larger system sizes. The true thermodynamic ODT must occur within the loops, but it is difficult to say exactly where. However, it is sensible to assume that the simulation time required to disorder a lamellar phase is significantly less than that required to form it,[19] and so we assume the thermodynamic ODT is towards the small χN end of the hysteresis loops. If we then exclude our smallest system sizes, which display an anomalously low $(\chi N)_{\mathrm{ODT}}$, we arrive at a fairly consistent value for the ODT of $(\chi N)_{\mathrm{ODT}}=40\pm 1$.

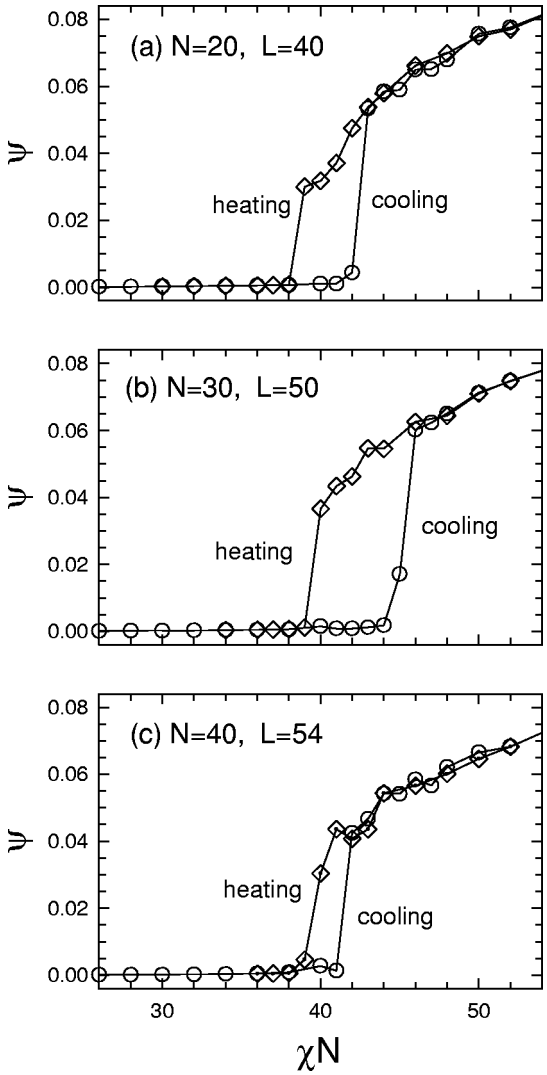

FIG. 6. Order parameter, ψ, from Monte Carlo runs where the system is cooled from $\chi N=0$ into the lamellar phase and then heated back into the disordered state. Results are presented for three degrees of polymerization: (a) $N=20$, (b) 30, and (c) 40.

D. Internal energy

Here, we compare the mean-field and Monte Carlo predictions for the internal energy, or equivalently the average number of AB contacts, since $U=\epsilon_{\mathrm{AB}}\langle n_{\mathrm{AB}}\rangle$ assuming that $\epsilon_{\mathrm{AA}}=\epsilon_{\mathrm{BB}}=0$. A sample of our Monte Carlo predictions are plotted in Fig. 7 for three different molecular weights. The molecular-weight dependence is largely removed by plotting the number of contacts versus χN. The plot shows a $\sim 60\%$ reduction in AB contacts as the ODT is approached ($\chi N \approx 40$), which is in stark contrast to the mean-field prediction, Eq. (41), suggesting a constant $\langle n_{\mathrm{AB}}\rangle/V=1.92$ throughout the disordered phase.

Not only does mean-field theory fail to capture the decrease in $\langle n_{\mathrm{AB}}\rangle$ as χN increases, it is highly inaccurate even in the athermal limit where $\chi N=0$. This is because mean-

TABLE II. Monte Carlo ODT's for three degrees of polymerization, N, each with four different system sizes, L.

	$(\chi N)_{\mathrm{ODT}}$			
N	$L=24$	$L=32$	$L=40$	$L=48$
20	37.0–37.0	40.5–42.5	38.5–42.5	39.5–43.5
	$L=30$	$L=40$	$L=50$	$L=60$
30	38.5–38.5	39.5–41.5	39.5–45.0	39.5–44.0
	$L=34$	$L=44$	$L=54$	$L=64$
40	37.5–37.5	40.5–43.5	38.5–41.5	38.5–43.5

field theory completely ignores the intramolecular correlations resulting from the connectivity of the chains, which act to shield a given monomer from contacts with other molecules. This so-called correlation hole effect[27] has been well studied in binary homopolymer blends.[28]

If we examine the ODT region carefully, discontinuous jumps in the internal energy are evident as observed earlier by Pakula *et al.*[16] and by Dotera and Hatano.[20] Furthermore, if we magnify the region and include both cooling and heating runs as in Fig. 7(b), we also find hysteresis loops consistent with the ones observed in the order parameter.

E. Heat capacity

The discontinuity in internal energy at the ODT should, in principal, produce a spike in the heat capacity, although earlier studies[13,15] have failed to detect one. However, consistent with the one documented exception by Pakula *et al.*,[16] we generally do observe a strong spike in the heat capacity in complete coincidence with the discontinuities in the internal energy and the order parameter. Figure 8 shows this spike for two equivalent and independent cooling runs. The slight shift in the two peaks is due to the small statistical variations in nucleating the lamellar phase. We also note that there can be considerable variation in the strength of the peak, and in some runs it is practically nonexistent. The explanation, however, is very simple. If the transition occurs completely within the equilibriating period immediately following a temperature step, the large energy fluctuations will not be captured by the statistical averaging [see Eq. (5)].

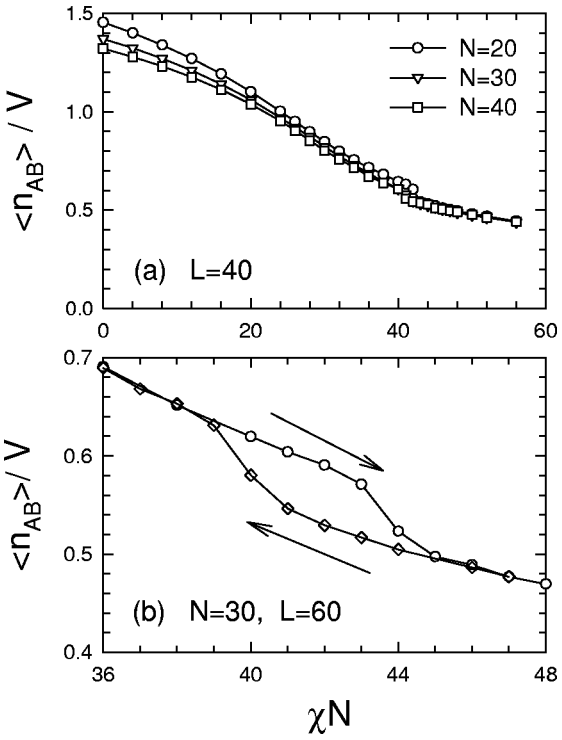

FIG. 7. (a) Average number of A/B monomer contacts, $\langle n_{\mathrm{AB}} \rangle$, vs segregation, χN, obtained from Monte Carlo cooling runs for three different molecular weights. (b) Hysteresis loop produced by cooling (○) and subsequent heating (◇) runs.

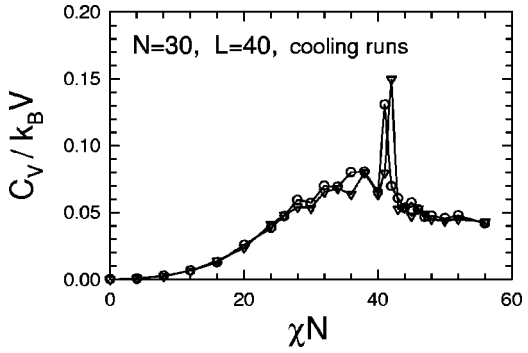

FIG. 8. Heat capacity, C_V, vs increasing segregation, χN, obtained from two statistically independent Monte Carlo runs for the same molecular weight, $N=30$, and the same system size, $L=40$.

F. Dimensions of an individual molecule

In an athermal melt (i.e., $\chi N=0$), polymer chains are expected to obey random-walk statistics with their dimensions scaling as $N^{1/2}$, consistent with the mean-field predictions in Eqs. (42)–(45). In practice though, fitting our radius of gyration to $R_g \propto N^{\nu}$ provides a somewhat larger exponent of $\nu=0.538$, agreeing with the values obtained by earlier studies.[10,12,21] Similarly, the A block radius of gyration, $R_{g\mathrm{A}}$, yields an exponent of $\nu=0.554$, and the block separation, R_{AB}, gives an exponent of $\nu=0.526$. Nevertheless, this minor deviation from $\nu=\frac{1}{2}$ is easily attributed to the fact our chains are not yet in the large-N regime.[10,12] Nevertheless, if we insist on fitting the radius of gyration to $R_g=a(N/6)^{1/2}$, we obtain an approximation for the statistical segment length of $a\approx 1.17b$, slightly larger than the mean-field prediction of $a=b$ [see Eq. (42)].

Figure 9 plots R_g, $R_{g\mathrm{A}}$, and R_{AB} relative to their mean-field predictions, Eqs. (42)–(45), as a function of χN. As found previously,[10–15,18] scaling the results in this manner is reasonably successful in collapsing the data onto a single curve. The fact that the $R_{g\mathrm{A}}$ results in Fig. 9(b) are somewhat spaced is just a consequence of the highly expanded vertical axis. Unlike most previous studies,[10–15,18] we observe small discontinuities at the ODT. In Fig. 9, we only display cooling curves, but if we included heating curves and increased the magnification, we would see small hysteresis loops consistent with the one in Fig. 7(b) for the internal energy.

Over the range of the disordered phase (i.e., $\chi N=0-40$), R_g increases by 7%–10%, but this does not repre-

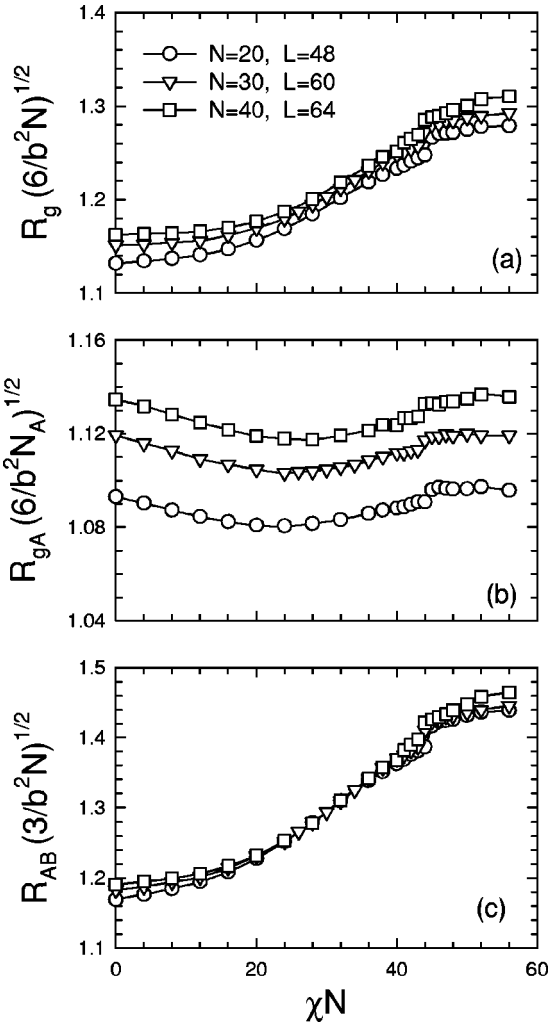

FIG. 9. (a) Radius of gyration of the entire molecule, R_g, (b) radius of gyration of the A block, R_{gA}, and (c) separation between the A and B block centers of mass, R_{AB}, plotted for increasing segregation, χN. Results are presented for $N=20$, 30, and 40 from simulations on lattices of $L=48$, 60, and 64, respectively.

sent a simple uniform stretching of the chains. Instead, it appears that the A and B blocks remain relatively uniform in size, while their centers of mass spread apart by 15%–18%. Previous studies[10,12,14,18] have likewise found that R_{AB} increases more than R_g. Interestingly, the individual blocks (in this symmetric case, the A and B blocks behave equivalently) seem to contract slightly when the temperature is first lowered,[11,14,15,29] consistent with calculations by Vilgis and Borsali[30] and analogous to Monte Carlo simulations on A + B homopolymer blends by Sariban and Binder.[31,32] However, we should be careful not to rule out the possibility that the blocks undergo a significant perturbation, since R_{gA} says nothing about their actual shape.

G. Correlation function

Since mean-field theory predicts that monomers are randomly mixed in the disordered phase, it follows that the spin–spin correlation function, G_{ij}, should be zero for any two sites $i \neq j$. However, our Monte Carlo simulations reveal a significant level of correlations in the disordered phase,

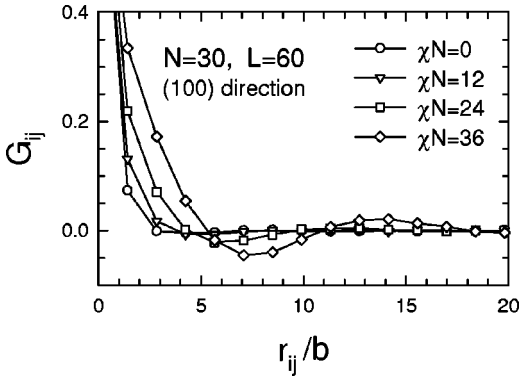

FIG. 10. Spin–spin correlation function, G_{ij}, vs separation, r_{ij}, between sites evaluated for a series of segregations within the disordered phase. In this case, the Monte Carlo simulations are performed on diblocks of $N=30$ monomers in a system of size $L=60$, and the separation between sites i and j is taken to lie along the (100) direction.

particularly as the ODT is approached. This is demonstrated in Fig. 10, where G_{ij} is plotted along the (100) direction as a function of separation, r_{ij}, for a series segregations. Although Larson[19] has reported the same damped oscillatory correlations, he did not investigate the effect of changing segregation. Here, we show that the length of the exponential-like decay and the wavelength of the oscillation both increase as the ODT is approached. The former indicates an increased level of microphase separation, while the latter is consistent with growth of the microdomains. This behavior is, in fact, a common feature of amphiphilic systems.[33]

H. Structure function

Figure 11(a) shows the spin–spin structure function at a series of segregations, χN, within the disordered phase. We follow the common practice of ignoring the slight dependence on orientation, and we average over all wave vectors of the same magnitude, $q \equiv |\mathbf{q}|$. The structure function exhibits a similar functional form to that predicted by mean-field theory,[6] but in this case the location of the peak shifts towards smaller wave vectors as the ODT is approached. The peak position, q^*, is plotted in Fig. 11(b) as a function of χN for three different molecular weights. As was the case for the average molecular dimensions, the molecular-weight dependence can be largely removed by scaling q^* with $N^{1/2}$. For completeness, we plot the peak height, $S(q^*)$, in Fig. 11(c), using a logarithmic scale so as to demonstrate its exponential-like growth.

The wavelength, $\lambda^* = 2\pi/q^*$, associated with the peak position, is related to the size of microdomains forming within the disordered phase. Over the range $\chi N = 0$ up to the ODT, λ^* increases almost linearly by approximately 40%. As Fried and Binder[10–12] have pointed out, this is much larger than the increase in either R_g and R_{AB}. It follows that the growth of microdomains in the disordered phase must be a highly cooperative process, as opposed to a simple consequence of chain stretching.

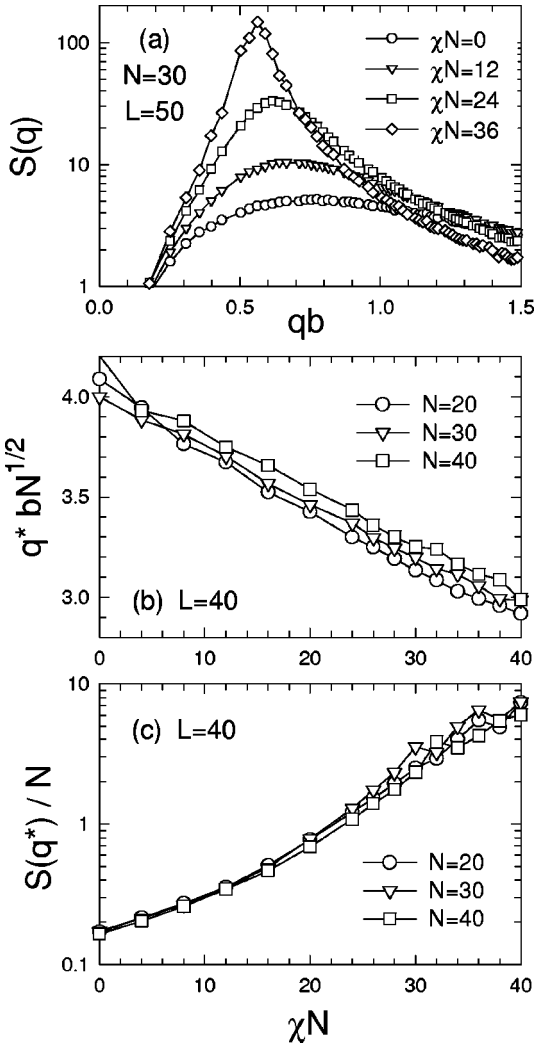

FIG. 11. (a) Spin–spin structure function, $S(q)$, vs wave number, q, for a series of segregations within the disordered phase. The simulations are performed on diblocks of $N=30$ monomers in a system of size $L=50$. (b) Wave number, q^*, and (c) height, $S(q^*)$, corresponding to the peak in the structure function plotted as functions of segregation for three different molecular weights.

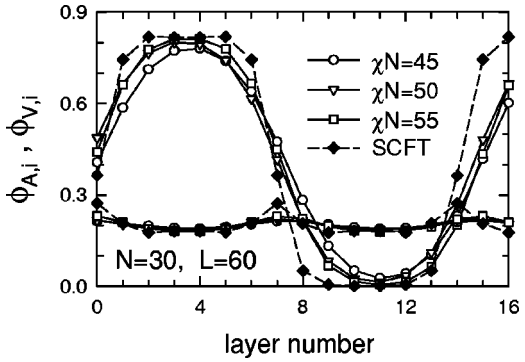

FIG. 12. Concentration profiles of A monomers and vacancies evaluated from a Monte Carlo cooling run involving diblocks of $N=30$ monomers in a system of size $L=60$ (open symbols). The vacancy profiles can be distinguished by the fact that $\phi_{V,i}\approx 0.2$. In this simulation, a (111) oriented lamellar phase formed during the latter MCS of $\chi N=43$ and the initial steps at $\chi N=44$ [see Figs. 5 and 7(b)]. For comparison, a mean-field prediction is shown for $\chi N=50$ (solid diamonds).

I. Lamellar profile

Figure 12 shows segment profiles of the lamellar phase at two segregations from the Monte Carlo cooling run corresponding to Figs. 5 and 7(b). On the basis of the hysteresis in Fig. 7(b) and the configuration in Fig. 5(d), the disordered state began to transform into a (111) lamellar state during $\chi N=43$ eventually reaching equilibrium by the end of the $\chi N=44$ step. The $\chi N=45$ profiles in Fig. 12 are the first from a fully equilibriated lamellar phase. As opposed to the mean-field behavior where the oscillatory profile grows in gradually (see Fig. 3), here it emerges abruptly consistent with a discontinuous ODT. As found previously by mean-field theory, the vacancy distribution remains reasonably uniform.

For comparison, we also display one mean-field profile in Fig. 12 calculated at $\chi N=50$. Mean-field theory predicts a period of $D=15$ layers which is just slightly shorter than the Monte Carlo result of $D=16$, but we should not associate any significance to this small discrepancy. First of all, the finite size of the simulation box precludes gradual increments in the Monte Carlo domain size, and secondly it is clearly evident from our simulations that nonequilibrium effects prevent the lamellar phase from adjusting to the continuously changing equilibrium period. Because of these finite-size and nonequilibrium effects, we forego any further investigation of the lamellar phase.

However, before moving on, it is interesting to note that the mean-field profile in Fig. 12 has a significantly sharper interface than those produced by the Monte Carlo simulations. This remains the case even when we perform the mean-field calculation at the same domain spacing of $D=16$. The explanation is very simple; mean-field theory ignores capillary wave fluctuations.[2,34] Past studies[35] have already demonstrated that correcting for this effect significantly improves the agreement between mean-field theory and Monte Carlo simulations. Contrary to the situation with the disordered phase, we conclude that mean-field theory appears reasonably accurate in describing the ordered lamellar phase, just as expected.[2]

V. DISCUSSION

In principle, comparisons between Monte Carlo simulations and mean-field theory offer a direct way of assessing fluctuation effects. However, this is only true if the comparison is performed using the same underlying model, which has not been the case. Monte Carlo simulations have been conducted on lattice models whereas mean-field theory has been performed on a continuum coarse-grained model. The comparison consequently requires some arbitrary judgement[21] for the definition of the Flory–Huggins χ parameter. We avoid this uncertainty by performing our mean-field calculations on the same identical lattice model used in our Monte Carlo simulations. With this ambiguity removed, the fluctuation effects can only be obscured by the statistical inaccuracies, finite-size effects, and nonequilibrium behavior in our Monte Carlo simulations, all of which we can deal with.

The statistical inaccuracies due to the finite sampling time in our simulations are easily assessed by examining the random noise in our various Monte Carlo data. In all cases, the visible noise is small relative to the measured quantities. Furthermore, we have confirmed the accuracy of our statistics by comparing a number of independent runs performed under identical conditions (see, for example, Fig. 8). If the accuracy was insufficient, it would only be a simple matter of collecting statistics over longer intervals.

The fact that simulations are performed on a finite lattice will naturally perturb the results away from the thermodynamic limit (i.e., $L\rightarrow\infty$). Such finite-size effects would be overwhelming if it was not for the periodic boundary conditions, but even with them the effects can be substantial. In general, the finite size of the simulation box tends to reinforce correlations thus promoting the stability of an ordered phase. In the case of binary homopolymer blends, this effect can be corrected for by finite-size scaling techniques allowing the ODT to be located to within $\sim$0.1% accuracy.[15] However, when the ordered phase is periodic, its formation is also affected by the fact that it must be commensurate with the finite size of the simulation box. Micka and Binder[15] concluded that this renders standard finite-size scaling techniques intractable, but fortunately the situation is not as bad as this suggests. Our mean-field calculations demonstrate that even large variations of $\pm$20% away from the preferred period only shift the ODT by $\sim$5% (see Fig. 2). Indeed, our Monte Carlo simulations predict reasonably consistent values of $(\chi N)_{\mathrm{ODT}}$ for all but our smallest system sizes.

Just as in experiment,[17,36] Monte Carlo simulations are prone to nonequilibrium effects due to the finite time the system spends at any given temperature. One result of the delayed response to a temperature increment is the hysteresis at a discontinuous transition.[17] In principle, the hysteresis loop should gradually shrink converging on the proper thermodynamic ODT as the system is equilibriated for longer periods of time,[36] but in practice the time required is often unfeasibly long. Fortunately, our hysteresis loops are small and furthermore we can be confident that the actual ODT is towards the low χN end of each loop, given that it is more difficult to form an ordered phase as opposed to melting it.[19] The fact that beyond the hysteresis our heating runs match up with our cooling runs (see, for example, Figs. 6 and 7) demonstrates that the disordered phase is free of nonequilibrium effects. On the other hand, we believe that the lamellar phase is overwhelmed by nonequilibrium effects in that once it forms the orientation and period are unable to adjust. For this reason, our investigation of fluctuation effects has avoided the lamellar phase. At any rate, mean-field theory is expected to be accurate for ordered phases, because the effective fields are relatively static.[2]

The remaining differences between mean-field theory and Monte Carlo can only be due to fluctuation effects. Some of these differences have already been established in previous Monte Carlo studies. For instance, the stretching of individual chains is virtually identical to that found by Binder and Fried.[10–12] Larson[19] has also observed oscillatory correlations similar to those in Fig. 10. The peak in the scattering function and the shift towards larger length scales with increasing χN are also well documented.[10–14,29] Although Micka and Binder[15] have shown that the average number of A–B monomer contacts, $\langle n_{\mathrm{AB}}\rangle$, decreases substantially as the ODT is approached, we are not aware of anyone pointing out the fact that mean-field theory is already considerably inaccurate in the athermal limit (i.e., $\chi N=0$). Even there, Eq. (41) overestimates the number of contacts in Fig. 7(a) by $\sim$35%.

Pakula *et al.*[16] claimed to identify a well-defined temperature at $\chi N\approx 0.7(\chi N)_{\mathrm{ODT}}$ separating mean-field and nonmean-field behavior. Not only do we detect significant fluctuation effects well below this segregation, none of our plotted quantities suggest any sort of crossover behavior whatsoever. On the basis of our uniform vacancy distribution in the lamellar phase (see Fig. 12) and past studies,[15,18,31] we doubt that this has anything to do with our use of vacancies. Indeed, our internal energy and specific heat curves show consistent behavior with theirs when plotted as a function of T rather than χN. This suggests that their evidence for a crossover is simply an artifact of how they plot their data. We note that this claim by Pakula *et al.* is very reminiscent of the proposed Gaussian to stretched-coil transition suggested by Bates *et al.*[37] based on their experimental plots of q^* versus N. In that case, Fried and Binder[12] have since provided compelling evidence that the observed behavior does not coincide with the onset of chain stretching.

Past studies have been unable to comment reliably on the quantitative effect of fluctuations on the ODT, because of difficulty in detecting the transition and the unavailability of mean-field predictions for their particular models. Now, for the first time, we are able to make accurate comparisons. For all three molecular weights considered in our study, the Monte Carlo simulations predict an ODT at $(\chi N)_{\mathrm{ODT}}=40\pm 1$, while mean-field theory predicts $(\chi N)_{\mathrm{ODT}}$ to range from 14.3 to 15.3 (see Tables I and II). Hence, mean-field theory underestimates $(\chi N)_{\mathrm{ODT}}$ by a factor of $\sim$2.7, and if anything the inaccuracy increases with molecular weight. Although previous studies[10,16,18,19] have not suggested an inaccuracy anywhere near as large, our result is not unprecedented. In Monte Carlo simulations for binary homopolymer blends, Sariban and Binder[31,32] have reported similar sized discrepancies that likewise show no sign of vanishing for large N.

It is unreasonable to expect the Fredrickson–Helfand fluctuation theory[3] to quantitatively apply to our results. Not only is the theory based on the continuum Gaussian chain model, but it also assumes $\bar{N}\gtrsim 10^6$ whereas our chains only range from $\bar{N}\approx 65$ to 130 (note that $\rho_0=\sqrt{2}\phi_c/b^3$ and $a\approx 1.17b$). Indeed, Eq. (1) predicts $(\chi N)_{\mathrm{ODT}}$ to increase by a factor of $\sim$1.8, which is significantly less than the $\sim$2.7 predicted by our study. (Note that we compare relative increases so as to avoid any direct comparison between the continuum and lattice definitions of χ.) Nevertheless, we do find that the ODT is discontinuous just as the F–H theory predicts. Furthermore, the F–H theory correctly predicts the ODT to shift towards higher χN, which incidentally contradicts the calculation by Maurer *et al.*[4]

Although the inaccuracy in the mean-field prediction of $(\chi N)_{\mathrm{ODT}}$ may eventually subside for larger N, it will never vanish in the $N\rightarrow\infty$ limit. The intramolecular correlations,

which persist even in the athermal limit, imply that the mean-field prediction for U, Eq. (41), will always be inaccurate. Some researchers[10,16,18] have partially corrected for this effect by replacing z by $(z-2)$ in Eq. (3) to account for the fact that a given monomer always remains in contact with its bonded neighbors. However, this is not a sufficient correction since the intramolecular correlations extend further than just one monomer along the chain. In many cases, this is accounted for by using an effective coordination number, which involves calculating the average number of nearest-neighbor sites blocked by intrachain contacts.[19]

The claim that mean-field theory becomes exact in the $N\rightarrow\infty$ limit can only be true for coarse-grained models. If we coarse grained our lattice model, defining segments each containing a reasonable number of monomers (i.e., 10 or more), then the intramolecular correlations would largely be confined to the individual segments and thus incorporated into an effective χ parameter describing the segment–segment interactions. Although there would always remain some intramolecular correlations between connected segments, these could be continuously reduced by making the segments ever larger. The resulting coarse-grained segments would differ substantially from our present monomers. The segments would instead behave like microscopic springs with a variable end-to-end length and they could overlap since they would no longer represent solid objects. However, this coarse-graining procedure could never be applied to polymers so short as the ones considered in our simulations, nor is it feasible to extend our simulations to sufficiently long polymers. Field-theoretic simulations[22] appear to be the only possible way of accessing the $N\rightarrow\infty$ limit, but it may be some time before the computational methods will be up to the challenge of performing accurate simulations in three dimensions.

VI. SUMMARY

We have expanded upon an earlier Monte Carlo study of diblock copolymer melts by Pakula *et al.*[16] The original study was one of only two to detect evidence of a discontinuous ODT, and the only one to suggest that fluctuation effects emerge at a well-defined temperature in the disordered state. Here, symmetric diblocks are examined for three molecular weights on a range of significantly larger system sizes in order to assess finite-size effects, and runs are performed for both cooling and heating. In addition to the internal energy, specific heat, and molecular size examined by Pakula *et al.*, we also investigated the shape of an individual chain, the correlation function, the structure function, and the lamellar profile. Furthermore, we have performed mean-field calculations on the same lattice model in order to provide the first direct and unbiased comparisons between Monte Carlo simulations and mean-field theory.

The nonmean-field behavior we observed in the disordered phase is consistent with previous Monte Carlo simulations[10–15] performed on a variety of lattice models. First of all, the behavior scales well with the product χN. Second, our results are consistent with the view that as χN increases the A and B blocks of each molecule gradually separate while remainly relatively uniform in size. Third, the A- and B-rich microdomains in the disordered phase grow faster than the dimensions of the individual molecules, demonstrating that microphase separation is a highly collective process.[10–12,15] Finally, we find that nonmean-field behavior begins immediately as χN increases from zero, and that there is no clear division between a homogeneous disordered state and a structured one contrary to the claim by Pakula *et al.*[16]

While most previous Monte Carlo studies[10–15] have failed to detect direct evidence of an ODT, we were able to locate it with relative ease. Furthermore, we could unambiguously identify it as a discontinuous transition based on the sudden jump it produced in all the thermodynamic quantities and the hysteresis loops observed when scanning back and forth across the ODT. The finite-size effects were found to be reasonably modest for all but our smallest system sizes, and thus we were able to provide a reliable estimate for the ODT, $(\chi N)_{\mathrm{ODT}}=40\pm1$. This was found to be $\sim$2.7 times our mean-field prediction calculated for the identical lattice model, a discrepancy much larger than that suggested by either the Fredrickson–Helfand fluctuation theory or any previous Monte Carlo study. We were also surprised to find that the inaccuracy in mean-field theory seems to increase for larger N. Although mapping large-N systems onto coarse-grained models will undoubtedly reduce some of this discrepancy, it still remains to be seen if mean-field theory becomes exact in the $N\rightarrow\infty$ limit.

ACKNOWLEDGMENTS

The authors are grateful to Marcus Müller for useful comments, and to the EPSRC (GR/N36721) and the Dow Chemical Company for financial support.

[1] F. S. Bates and G. H. Fredrickson, Phys. Today **52**, 32 (1999).
[2] M. W. Matsen, J. Phys.: Condens. Matter **14**, R21 (2002).
[3] G. H. Fredrickson and E. Helfand, J. Chem. Phys. **87**, 697 (1987).
[4] W. W. Maurer, F. S. Bates, T. P. Lodge, K. Almdal, K. Mortensen, and G. H. Fredrickson, J. Chem. Phys. **108**, 2989 (1998).
[5] S. A. Brazovskii, Sov. Phys. JETP **41**, 85 (1975).
[6] L. Leibler, Macromolecules **13**, 1602 (1980).
[7] F. S. Bates, M. F. Schulz, A. K. Khandpur, S. Förster, J. H. Rosedale, K. Almdal, and K. Mortensen, Faraday Discuss. **98**, 7 (1994).
[8] A. Kudlay and S. Stepanow, J. Chem. Phys. **118**, 4272 (2003).
[9] K. Binder and M. Müller, Curr. Opin. Colloid Interface Sci. **5**, 315 (2000).
[10] H. Fried and K. Binder, J. Chem. Phys. **94**, 8349 (1991).
[11] K. Binder and H. Fried, Macromolecules **26**, 6878 (1993).
[12] H. Fried and K. Binder, Europhys. **16**, 237 (1991).
[13] A. Hoffmann, J.-U. Sommer, and A. Blumen, J. Chem. Phys. **107**, 7559 (1997).
[14] A. Hoffmann, J.-U. Sommer, and A. Blumen, J. Chem. Phys. **106**, 6709 (1997).
[15] U. Micka and K. Binder, Macromol. Theory Simul. **4**, 419 (1995).
[16] T. Pakula, K. Karatasos, S. H. Anastasiadis, and G. Fytas, Macromolecules **30**, 8463 (1997).
[17] D. A. Hajduk, S. M. Gruner, S. Erramilli, R. A. Register, and L. J. Fetters, Macromolecules **29**, 1473 (1996).
[18] A. Weyersberg and T. A. Vilgis, Phys. Rev. E **48**, 377 (1993).
[19] R. G. Larson, Macromolecules **27**, 4198 (1994).
[20] T. Dotera and H. Hatano, J. Chem. Phys. **105**, 8413 (1996).
[21] Q. Wang, P. F. Nealey, and J. J. de Pablo, Macromolecules **35**, 9563 (2002).
[22] V. Ganesan and G. H. Fredrickson, Europhys. Lett. **55**, 814 (2001); G. H. Fredrickson, V. Ganesan, and F. Drolet, Macromolecules **35**, 16 (2002).
[23] J. M. H. M. Scheutjens and G. J. Fleer, J. Phys. Chem. **83**, 1619 (1979).
[24] J. R. Naughton and M. W. Matsen, Macromolecules **35**, 5688 (2002).

[25] D. P. Landau and K. Binder, *A Guide to Monte Carlo Simulations in Statistical Physics* (Cambridge University Press, Cambridge, 2000).
[26] P. J. Flory, *Principles of Polymer Chemistry* (Cornell University Press, New York, 1953), pp. 428–430.
[27] P.-G. de Gennes, *Scaling Concepts in Polymer Physics* (Cornell University Press, New York, 1979), pp. 62–68.
[28] M. Müller and K. Binder, Macromolecules **28**, 1825 (1995).
[29] W. H. Jo and S. S. Jang, J. Chem. Phys. **111**, 1712 (1999).
[30] T. A. Vilgis and R. Borsali, Macromolecules **23**, 3172 (1990).
[31] A. Sariban and K. Binder, Macromolecules **21**, 711 (1988).
[32] A. Sariban and K. Binder, J. Chem. Phys. **86**, 5859 (1987).
[33] G. Gompper and M. Schick, *Self-Assembling Amphiphilic Systems* (Academic, London, 1994).
[34] A. N. Semenov, Macromolecules **26**, 6617 (1993); K. R. Shull, A. M. Mayes, and T. P. Russell, *ibid.* **26**, 3929 (1993).
[35] A. Werner, F. Schmid, and M. Müller, J. Chem. Phys. **110**, 5370 (1999); T. Geisinger, M. Müller, and K. Binder, *ibid.* **111**, 5251 (1999).
[36] D. A. Hajduk, H. Takenouchi, M. A. Hillmyer, F. S. Bates, M. E. Vigild, and K. Almdal, Macromolecules **30**, 3788 (1997).
[37] K. Almdal, J. H. Rosedale, F. S. Bates, G. D. Wignall, and G. H. Fredrickson, Phys. Rev. Lett. **65**, 1112 (1990).